Nanoscale Advances

ROYAL SOCIETY OF CHEMISTRY

PAPER

View Article Online
View Journal | View Issue

Cite this: *Nanoscale Adv.*, 2025, **7**, 467

Interaction of Langmuir–Blodgett films of Mn_{12} single molecule magnets with superconducting micro-tracks and nano-SQUIDs†

Bibekananda Das, ‡*[a] Tapas Senapati, ‡[a] Malaya K. Sahoo, [b] Jogendra N. Behera *[bc] and Kartik Senapati *[ac]

Molecular magnets with large spin moments are promising spintronic materials. In this report we study the feasibility of integrating these molecules into the field of superconducting spintronics which essentially deals with the mutual interactions of magnetic and superconducting systems. In this regard we have done two separate experiments using the widely studied single molecule magnet (SMM) Mn_{12}-ac. By performing transport measurements on thin superconducting micro-tracks of Nb coated with a Langmuir–Blodgett film of the Mn_{12}-ac SMM, we show that the SMM film significantly enhances the vortex activation energy near the transition temperature. The SMM can, therefore, help tuning the operating conditions of superconducting transition edge sensors. In a separate experiment, a Langmuir–Blodgett film of the SMM was grown onto a superconducting Nb nano-SQUID to look for local changes in magnetization arising from the magnetization tunneling phenomenon in the SMM. We observe random jumps in the voltage across the nano-SQUID corresponding to changes in the magnetization state of the SMM near the SQUID loops, which were not observed in the nano-SQUID without the SMM. These experiments show that the large spin moment and the discrete relaxation of magnetization in molecular magnets can be utilized to generate measurable signals in superconducting spintronic devices.

Received 15th August 2024
Accepted 20th November 2024

DOI: 10.1039/d4na00672k

rsc.li/nanoscale-advances

Introduction

In recent years, single molecule magnets (SMMs) have gained a lot of attention because of their potential application in the fields of molecular spintronics and quantum computing.[1–4] Among various SMMs, Mn_{12}-acetate (Mn_{12}-ac) is the most widely studied system which was first synthesized by Lis *et al.*[5] The chemical formula of the Mn_{12}-ac crystal is given by $[Mn_{12}O_{12}(CH_3COO)_{16}(H_2O)_4]\cdot 2CH_3COOH\cdot 4H_2O$. The molecule consists of four Mn^{4+} and eight Mn^{3+} ions coupled *via* super-exchange interaction through oxygen bridges. These high spin ($S = 10$) molecules undergo slow, thermally driven magnetic-relaxation because of a strong magnetic anisotropy barrier between the two easy magnetization directions. Below a characteristic blocking temperature ($T_B \sim 4$ K), these molecules also exhibit quantum tunneling of magnetization (QTM).[6–9] For spintronic applications it is imperative to obtain thin films of these molecules. Therefore, several techniques have been employed to prepare SMM thin films such as drop & dry,[10,11] dip & dry,[12] laser ablation,[13] *etc.* While the drop & dry technique suffers from accumulation of large non-uniform aggregations, the laser ablation technique runs the risk of structural damage to the molecules due to the exposure to high laser energy. The Langmuir–Blodgett (LB) technique is another film growth technique which overcomes both the above issues and results in a controlled layer growth.[14–16] LB films of Mn_{12}-ac have been grown by mixing it with behenic acid (BA) lipid ($C_{21}H_{43}COOH$).[14,17,18] In the dilute thin film form, however, the characteristic response of the SMM system is different from the bulk SMM crystals and aggregates.[7,10–12,14]

The purpose of this manuscript is to examine the feasibility of generating a measurable effect on the critical parameters of a superconducting film or device by a vicinal low density SMM film. The opposite effect, *i.e.* the effect of superconducting transition on the magnetization dynamics of a SMM film in the SMM/superconductor bilayer system, has been examined by Serrano *et al.*[19] They have shown that the superconducting transition of a Pb (111) crystal leads to a disruption of the blocked state of the Fe_4 SMM film grown on the Pb surface. The Fe_4 SMM film, in the work of Serrano *et al.*, was grown *via*

[a]*School of Physical Sciences, National Institute of Science Education and Research (NISER) Bhubaneswar, An OCC of Homi Bhabha National Institute, Jatni-752050, Odisha, India. E-mail: bibekanandadas404@gmail.com; kartik@niser.ac.in*

[b]*School of Chemical Sciences, National Institute of Science Education and Research (NISER) Bhubaneswar, An OCC of Homi Bhabha National Institute, Jatni-752050, Odisha, India. E-mail: jnbehera@niser.ac.in*

[c]*Center for Interdisciplinary Sciences (CIS), National Institute of Science Education and Research (NISER), An OCC of Homi Bhabha National Institute (HBNI), Jatni-752050, Odisha, India*

† Electronic supplementary information (ESI) available. See DOI: https://doi.org/10.1039/d4na00672k

‡ These authors contributed equally to this work.

thermal sublimation, which formed large patches of hexagonally packed films. Below the critical field of the superconducting crystal, the local penetration of the external magnetic field led to the breaking of the correlated blocking of magnetization in the Fe_4 SMM patches. It is, therefore, a natural question to ask that whether the magnetic flux emanating from the molecular magnet can lead to a change in the critical parameters of a nearby superconducting film or device. Earlier, a Josephson junction has been used as a detector of electromagnetic radiation emitted during magnetization avalanches of the Mn_{12}-ac crystal.[20] Bellido *et al.* deposited Mn_{12}-benzoate inside a SQUID loop using the dip-pen nanolithography technique to measure its ac susceptibility.[21] In this context, here we have studied the vortex activation energy and critical temperature of Nb micro-tracks coated with a low density LB film of Mn_{12}-ac molecular magnets. By comparing the transport data of SMM coated Nb tracks with bare Nb tracks we show that the presence of a SMM film on the superconducting tracks indeed imparts a small but measurable change in the dynamics of magnetic vortices in the Nb tracks. Similarly, by studying the time response of the voltage across a Mn_{12}-ac coated Nb nano-SQUID we show a possible signature of magnetization tunneling in Mn_{12}-ac, as a voltage jump corresponding to a sudden change in the local moment in the vicinity of the nano-SQUID loop.

Experimental section

Preparation of magnetic Mn_{12}-ac powder

The Mn_{12}-ac powder was prepared[22] by mixing 4.0 g of manganese acetate tetrahydrate ($Mn(CH_3COO)_2 \cdot 4H_2O$) with 40 mL of 60% acetic acid, which was stirred continuously until all the manganese acetate was completely dissolved. Thereafter, 1.0 g fine powder of $KMnO_4$ was added slowly for 2 min and then the resulting solution was further stirred for about 2 min. Afterwards, the solution was kept undisturbed for 3 days and thereafter the solution was filtered and washed with acetone repeatedly and dried at room temperature in a vacuum oven overnight and stored for further use. The vibrational spectra of functional groups of the as prepared Mn_{12}-ac powder and the purchased BA powder were recorded using Fourier transform infrared (FTIR) spectroscopy [ESI Fig. S1†]. The variation of magnetization (M) of the powdered form of Mn_{12}-ac clusters with the magnetic field and temperature has been studied using a vibrating sample magnetometer (VSM). The temperature dependent magnetization of the powder, $M(T)$, was recorded to ascertain the characteristic magnetic behavior of Mn_{12}-ac.

Lithographic patterning of Nb micro-tracks and Nb nano-SQUIDs

Two μm wide tracks with current and voltage contacts were first patterned on photoresist films, spin-coated on a Si/SiO_2 substrate, using the UV photo-lithography technique. These patterned substrates were then loaded in a high vacuum chamber with base pressure $\sim 5 \times 10^{-8}$ mbar. Thin Nb films were then deposited using the DC magnetron sputtering technique at room temperature[23] on these patterned substrates at an argon pressure of 1×10^{-2} mbar, while rotating the substrate under the target for uniform deposition. Subsequent to the deposition of the film, 2 μm Nb tracks with electrodes were developed by lifting off the photoresist in acetone. An optical image of the resulting pattern is shown in Fig. 1(a). For studying the effect of the high spin magnetization of the SMM on the critical parameters of the superconducting micro-tracks, SMM layers were deposited directly on these patterned films by the LB method. Prior to the deposition of the SMM layers, the superconducting critical parameters of the as grown Nb micro-tracks were measured in the temperature range of 2 K to 8 K.

For the second part of the experiment, aimed at detecting signatures of magnetization tunneling of SMMs, nano-SQUID devices were fabricated on separate Nb micro-tracks using a commercial focused ion beam milling (FIB) system. As shown in Fig. 1(b), the high energy (30 keV) focused ion beam was used to cut a deep trench of width $\sim$ 40 nm across the 2 μm track, leaving only two narrow bridge-like contacts across the Nb electrodes. The diameter of the nano-SQUIDs, formed in this process, was $\sim$40 nm. In this case also the magnetic field response of the nano-SQUIDs prior to the deposition of the SMM layers was compared with the post deposition response. The dimensions of both the weak links were kept close to the coherence length of Nb which also avoided any hysteretic behaviour in the *I–V* characteristics.[24] The loop inductance was calculated to be 0.014 pH. For the small junctions kinetic inductance of the loop can dominate over loop inductance.[25] By considering (penetration depth $\lambda = 120$ nm), the kinetic inductance for each junction was found to be ($L_{KE} = \mu_0\lambda^2 l/wt$) 1.13 pH where l, w, and t represent the length, width and thickness of the weak link, respectively.[26,27] Therefore, the fabricated nano-SQUID devices had a screening parameter $\beta_L \ll 1$, and the constricted Nb within the coherence limit provides the necessary condition for non-hysteretic *I–V* measurements.[28,29]

Deposition of the Langmuir–Blodgett film on Nb micro-tracks and Nb nano-SQUIDs

The LB technique was used to coat the SMM in a layer by layer fashion. Hydrophilic Mn_{12}-ac molecules do not form a stable Langmuir film upon spreading on the water surface. Therefore, an amphiphilic matrix is required which can hold Mn_{12}-ac molecules on the water surface. BA has been used earlier as a matrix to form stable LB films of Mn_{12}-ac.[14,17,18] The amphiphilic BA molecule consists of a hydrophilic head and a hydrophobic tail, as shown schematically in Fig. 1(c). A solution of BA and Mn_{12}-ac was prepared in chloroform ($CHCl_3$) in order to spread on the water surface. The schematic of linking of hydrophilic heads of the BA molecules to a Mn_{12}-ac molecule inside $CHCl_3$ is shown in Fig. 1(c). We note here that the Mn_{12}-ac molecule is much larger than the hydrophilic head of the BA molecule and, multiple BA molecules attach to a single Mn_{12}-ac molecule in the $CHCl_3$ solution. Upon dispersal of the solution on a Langmuir trough the hydrophobic tails of BA molecules holding the SMMs remain above the water surface, as shown in

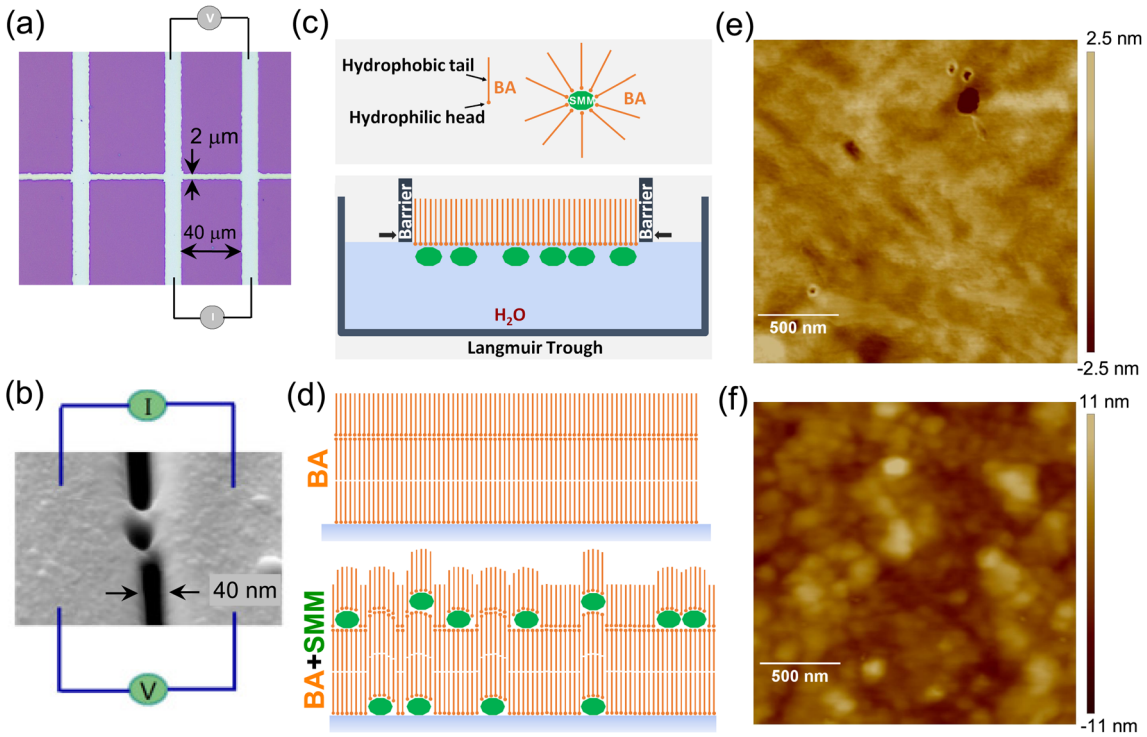

Fig. 1 (a) Optical image of a lithographically patterned Nb track of width 2 μm and thickness of 18 nm on a Si/SiO_2 substrate. The configuration of four probe transport measurement leads is also indicated. (b) Scanning electron micrograph of a focused ion beam patterned Nb nano-SQUID showing a SQUID loop of ~40 nm diameter. This device was fabricated from a 45 nm thick Nb film. (c) Schematic of a behenic acid (BA) molecule with a hydrophobic tail & hydrophilic head (top left), linking of BA molecules to a single Mn_{12}-ac molecule in chloroform (top right), and the Langmuir film of a mixture of BA & Mn_{12}-ac on the water surface in the Langmuir trough (bottom). (d) Schematic of the periodic arrangement of Langmuir–Blodgett BA layers (top) and BA–SMM–BA layers on the substrate surfaces (bottom). (e and f) show the atomic force microscopy images of 15 MLs of a LB film of BA and SMM intercalated BA deposited on Si/SiO_2, respectively.

Fig. 1(c). Since the Langmuir film is essentially formed by the lipid (BA) molecules, which carry the Mn_{12}-ac molecule, upon dispersal in water the Mn_{12}-ac molecules naturally get arranged separated from each other. This is unlike the films obtained by the thermal sublimation method employed by Serrano *et al.*,[19] where the SMMs were arranged in a hexagonally packed form. A Langmuir trough (model KSV NIMA) with two symmetrical barriers has been used to prepare the Langmuir films. The width and area of the trough were 75 mm and 24 300 mm^2, respectively. A Pt Wilhelmy plate has been used as a balance to sense the surface pressure[30] which was kept perpendicular to the barrier. The trough and Pt plate have been cleaned with 2-propanol and Milli-Q water before use. Before the growth of the LB film, we have tested the complete isotherm and the details have been given in the ESI (Fig. S2(a)).† Nb micro-tracks or Nb nano-SQUIDs fabricated on Si/SiO_2 have been immersed inside the Milli-Q water subphase before spreading of the Mn_{12}-ac/BA solution. BA and Mn_{12}-ac with a concentration of 10^{-3} M : 10^{-4} M ratio were added to volatile $CHCl_3$ chosen as the spreading agent. The prepared mixture of the BA & SMM solution was homogeneously spread dropwise throughout the subphase using a 50 μL micro-pipette. The system was kept undisturbed for 20 min for the evaporation of $CHCl_3$ from the surface of the subphase. Then, the two symmetric barriers were compressed with a constant speed of 3 mm min^{-1} to achieve the desired surface pressure of 30 mN m^{-1}, where the Mn_{12}-ac/BA film was found to be in the solid monolayer phase and the film was kept for 30 min before deposition. The barriers were moved to and fro at a constant speed of 3 mm min^{-1} to get a stabilized Langmuir film. After waiting for 30 min, the Langmuir film was transferred to the substrate (within Nb micro-tracks or Nb nano-SQUIDs) by lifting the dipper with a speed of 1 mm min^{-1}. The film was then dried for 30 min well above the water surface before dipping again for deposition of the next layer on top of the first layer. Fig. S2(b)† shows an optical image of a LB film of a mixture of BA & SMM deposited on a patterned Nb layer. Fig. 1(d) shows the schematic arrangement of a BA film and the Mn_{12}-ac intercalated BA film. Atomic force microscopy (AFM) in non-contact mode and low angle X-ray reflectivity techniques have been used to study the arrangement of Mn_{12}-ac intercalated BA layers. The point to note here is that the Mn_{12}-ac molecules remain separated from each other inside the BA matrix when deposited on the Nb tracks and the Nb nano-SQUIDs.

Electrical characterization of SMM coated Nb micro-tracks and Nb nano-SQUIDs

In order to study the effect of magnetic flux of Mn_{12}-ac on the superconducting properties of a thin Nb micro-track, we performed electrical transport measurements before and after

deposition of the SMM layer on the micro-tracks. All transport measurements were performed in a four probe geometry, as shown in Fig. 1(a). Magnetic fields were applied perpendicular to the surface of micro-strips in order to study the magnetic vortex activation process below the superconducting transition temperature. The nano-SQUIDs were also connected in a four probe geometry as shown in Fig. 1(b), and the characteristic field response of the bare nano-SQUIDs was compared with that of the SMM coated nano-SQUIDs. SQUIDs were biased at a constant current and the voltage across the SQUID was recorded as a function of time for both types of samples in order to identify features corresponding to magnetization tunneling in SMMs.

Results and discussion

We have arranged this section in the following manner. First we discuss the magnetic characteristics of the Mn_{12}-ac powder we have prepared in order to ascertain the quality of the starting material. We then discuss the structural characteristics of the Mn_{12}-ac SMM intercalated BA films on bare substrates and on the Nb surface. We note here that, by construction, the films formed by the LB method carry a very low density of Mn_{12}-ac, embedded in the BA matrix. We have resorted to the comparison of surface morphology and X-ray reflectivity (XRR) of bare BA films with those of the Mn_{12}-ac intercalated BA films to get indirect evidence of the intercalated molecules. After structural confirmation, we discuss the effect of SMMs on the superconductivity in the Nb micro-tracks. Finally, we discuss the nano-SQUID response in the presence of a LB coated SMM film.

Magnetic properties of Mn_{12}-ac powder

Fig. 2(a) shows the magnetic field dependent magnetization $M(H)$ of the as prepared Mn_{12}-ac powder, measured at several temperatures close to the blocking temperature. The hysteresis loop of Mn_{12}-ac is believed to be driven by the long magnetization relaxation times[6] of the molecules below a characteristic blocking temperature. Consistent with the earlier report,[22] the hysteresis vanished above the blocking temperature, as shown in Fig. 2(a). The inset in Fig. 2(a) shows a comparison of magnetic hystereses of the Mn_{12}-ac powder at a fixed temperature (2.7 K), measured at two different sweep rates (0.05 T min^{-1} and 0.2 T min^{-1}) of the magnetic field. As expected for a typical bulk SMM system, the slower measurement resulted in a smaller hysteresis. The steps in the hysteresis loops measured below the blocking temperature represent a magnetic avalanche

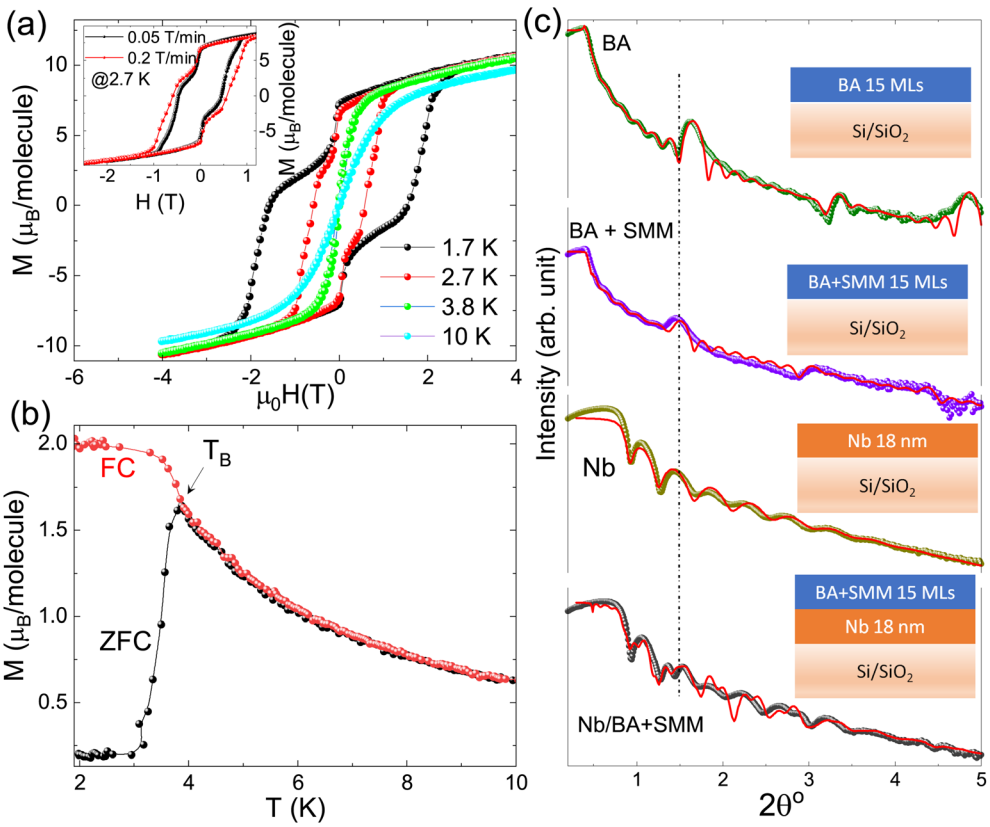

Fig. 2 (a) Magnetic hysteresis loops of Mn_{12}-ac powder measured at different temperatures showing characteristic steps corresponding to magnetization tunneling below 3 K. The inset compares the magnetization loops measured at different field sweep rates (0.05 T min^{-1} & 0.2 T min^{-1}) at 2.7 K indicating slow relaxation of SMMs. (b) Zero-field cooled (ZFC) and field-cooled (FC) temperature-dependent magnetization of Mn_{12}-ac powder measured at 0.1 T showing the blocking temperature marked as T_B. (c) Low angle X-ray reflectivity patterns of 15 monolayers (MLs) of a BA film, 15 MLs of a mixture of BA & SMM films, a Nb film, and a Nb film with 15 MLs of a mixture of BA & SMM films deposited on Si/SiO_2 substrates. The solid curves are the simulated curves.

triggered by quantum tunneling of magnetization (QTM).[7] At 1.7 K, steps in magnetization can be observed at three different fields (obtained from the dM/dH *vs.* H curve not shown here) ~0.023, ~1.97 and ~2.3 T. The hysteresis behavior vanishes above 4 K because thermal energy surpasses the anisotropy barrier for the magnetization. Fig. 2(b) shows the zero-field cooled (ZFC) and field-cooled (FC) temperature-dependent magnetization $M(T)$ measured with a magnetic field of 0.1 T. The peak in the ZFC curve at a temperature close to ~4 K gives a direct measure of the blocking temperature, consistent with the results in Fig. 2(a). Only after confirming the expected magnetic behavior of the prepared SMM powder, it was used for the formation of LB films on the superconducting micro-tracks and on nano-SQUID devices.

Structural characterization of Mn_{12}-ac multilayers deposited on the Nb surface

The comparison of AFM 2D images given in Fig. 1(e) and (f) shows that the SMM intercalated BA film has granular surface morphology with a root mean square (RMS) roughness of ~2.6 nm as compared to the smooth flat topography of the BA film with a RMS roughness of ~0.4 nm. This indicates that the SMM has been intercalated between BA layers. Additionally, non-destructive specular low-angle XRR is an efficient technique to study the arrangement of molecules in the LB film.[31] The top panel of Fig. 2(c) shows the low angle XRR for a 15-layer, bare BA film (which is the amphiphilic matrix supporting the Mn_{12}-ac molecules on the water surface) deposited directly on the Si/SiO_2 substrate. The diffraction pattern consists of Bragg's peaks of the periodic arrangement of BA layers with one bilayer (corresponding to one full cycle of downward and upward movement of the LB dipper) as one unit cell,[32,33] along with subsidiary peaks in between.[33] The 15-monolayer (ML) film of BA (equivalent to 7.5 unit cells) is expected to have a maximum of $7.5 - 2 = 5.5$ subsidiary peaks on both sides of the Bragg peaks.[32,33] In this case, there are 5 and 6 subsidiaries seen on the left and right hand side of the Bragg peak at 1.63°. Such XRR patterns have been reported earlier in the LB film of a mixture of stearic acid with 1-pyrene-dodecanoic acid,[32] and with Mn-stearate.[33] The XRR simulation yields the periodicity of about 5.4 nm for BA which is close to the reported periodicity of LB films of BA.[14] In addition, the XRR fitting parameters also yielded a total thickness of the film, which was found to be ~40 nm with each layer roughness less than 1 nm. The XRR pattern of 15 MLs of a mixture of BA & Mn_{12}-ac deposited on Si/SiO_2 is similar to that of 15 MLs of a bare BA film deposited on Si/SiO_2. However, the Bragg peak of periodic arrangement of BA has been shifted from 1.63° to 1.45° indicating intercalation of the Mn_{12}-ac molecules between two BA layers, as schematically shown in Fig. 1(d). The simulated curve yields the periodicity of the two BA layers separated by a Mn_{12}-ac layer to be ~6 nm with a layer roughness of less than 1 nm and total thickness of ~45 nm. The Mn_{12}-ac molecule is a disc like structure with 1.6 nm diameter and 1.1 nm height.[34] The observed periodicity (6 nm) of the SMM intercalated BA layers is, therefore, quite less than the expected value of 6.5 nm. This indicates that the Mn_{12}-ac molecules do not form a continuous layer in between two BA layers and the resulting SMM intercalated BA films have a very low density of the SMM. This is possibly due to the fact that each Mn_{12}-ac molecule attaches to several BA molecules in the chloroform solution, as shown in the schematic in Fig. 1(c). When dispersed on the water surface in the Langmuir trough the BA molecules open up to allow hydrophobic ends to stay above the water surface. As a result the separation between the individual SMM molecules naturally increases, forbidding a continuous film of SMMs in this method.

The same XRR experiment was also performed on the Nb films, instead of bare Si/SiO_2 substrates, as shown in the third and fourth panels of Fig. 2(c). From the fittings (shown as solid curves), the thickness of the Nb film was determined to be ~18 nm. When the SMM intercalated BA film was deposited on the Nb film, the XRR measurements did not show all the subsidiary peaks, unlike the Si/SiO_2 substrates. This is due to the dominance of diffraction intensity from the metallic Nb film over the SMM intercalated BA film. The position of the Bragg peaks for the 15-layer SMM intercalated BA film deposited on Nb, however, appeared to match with that of the SMM intercalated BA film deposited on Si/SiO_2.

Enhanced pinning in Mn_{12}-ac coated superconducting Nb micro-tracks

Fig. 3(a) shows the comparison of temperature-dependent resistances ($R(T)$) of a 2 μm wide Nb track before and after the deposition of a 21 MLs LB film of Mn_{12}-ac. The T_C of an 18 nm bare Nb micro-track was ~6 K as the thickness of the Nb film is less than the coherence length of Nb.[35–38] It is evident from Fig. 3(a) that the proximity of the Mn_{12}-ac SMM layer decreases the T_C of the same Nb micro-track to some extent. In fact we have found that increasing thickness of the Mn_{12}-ac SMM layer gradually decreases the T_C of the Nb track [data shown in ESI Fig. S3†]. The insets of Fig. 3(a) show the $R(T)$ curves of a Nb micro-track in the presence of various magnetic fields applied perpendicular to the film plane, before and after coating with Mn_{12}-ac SMMs.

In type-II superconductors, magnetic vortices play an important role in the superconductor to normal transition region. Specifically, thermal activation of magnetic vortices causes an Arrhenius type temperature dependence[39] of the resistance $R(T,H) = R_0 e^{-U/k_B T}$, near to the transition. Here R_0 is a pre-exponential factor and U is the activation energy required for the magnetic vortices to overcome the pinning barriers.[39–43] In the insets in Fig. 3(b) we have shown the Arrhenius plots ($\ln R$ *vs.* $1/T$ plots) for resistances near the normal-to-superconductor transition, measured with perpendicular magnetic fields up to 2 T. The red-solid lines are the linear fits in the transition region. From the slope of these fits the vortex activation energies (U) of Nb tracks have been calculated with and without the SMM coating. In both cases, the activation energy U was found to decrease with increasing magnetic field strength, as shown in the main panel of Fig. 3(b). However, it is evident from Fig. 3(b) that U of SMM coated Nb tracks is higher than that of the bare Nb track, up to ~0.6 T. Above this field, the activation energies

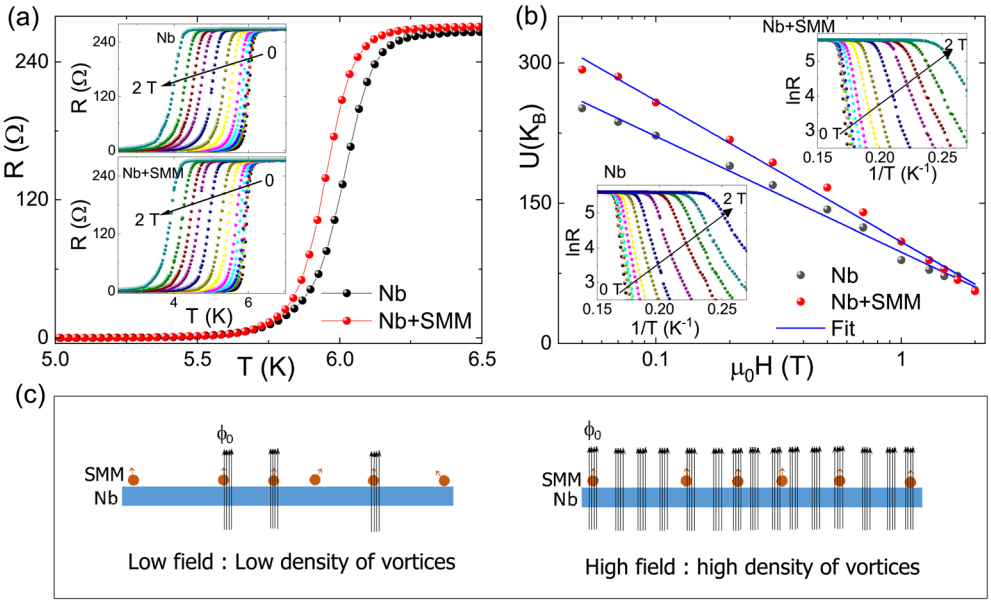

Fig. 3 (a) Temperature-dependent resistance $R(T)$ of a bare Nb track & SMM coated Nb track at 0 T and at different magnetic fields (see insets). (b) Field dependence of U of bare Nb and SMM coated Nb micro-tracks. The solid lines are the fits to eqn $U \propto \ln H$. The insets show the Arrhenius plots of resistance ln R *vs.* $1/T$ at different magnetic fields and the solid lines are the linear fits. (c) Schematic cross-sectional view of penetrating vortices in the low and high field conditions for SMM coated Nb tracks.

are similar for both cases, within experimental uncertainty. The magnetic field penetrates a type-II superconducting film as quantized flux ϕ_0 (2.07×10^{-7} G cm^2) bundles at random locations. The high spin magnetic molecules in the SMM film on top of the superconducting Nb act as trapping points for the entering vortices, as shown in Fig. 3(c). As a result, the overall motion of the network of vortices is restricted to some extent, which appears as an enhancement in the activation energy of the SMM coated Nb film seen in Fig. 3(b). On the other hand, at higher fields, when the density of magnetic vortices exceeds the number density of SMMs (shown in Fig. 3(c)), the overall response of the SMM coated Nb film approaches that of the bare Nb. The field dependent activation energy plotted in Fig. 3(b) fitted well with the empirical relation $U = U_0 \ln(H_0/H)$, where U_0 is a characteristic vortex unbinding energy and $H_0 \simeq H_{C_2}$ (upper critical field).[40,43,44] In our experiment, the Mn_{12}-ac magnetic molecules are embedded within the behenic acid layers. Therefore, the SMM can interact with the superconducting film *via* the magnetic flux emanating from the SMM. The fact that the superconducting film and the superconducting SQUID devices can respond to this magnetic flux from SMMs, without direct contact with the molecule, is actually a key aspect of combining these two types of materials. The experimental results, presented in this manuscript, have essentially demonstrated the feasibility of such magnetic flux based interaction between SMMs and superconducting films.

Observing the signature of magnetization tunneling in Mn_{12}-ac coated Nb nano-SQUIDs

In Fig. 4(a) we compare the $R(T)$ of the fabricated nano-SQUID device with and without the SMM coating. The resistance was measured at 0.1 μA current while warming from the lowest measurable temperature. The T_C of nano-SQUIDs remains unaffected (7.7 K) after the deposition of the LB Mn_{12}-ac film. This indicates that the magnetic moment of SMMs is practically ineffective for reducing the T_C of a 45 nm thick Nb film. This is unlike the case discussed in the previous section, where the Nb film was intentionally kept much thinner (18 nm) than the coherence length of Nb to detect a response of the SMM layer.

We also compared the magnetic field responses of the same nano-SQUID device at 2 K, before and after SMM coating, as shown in Fig. 4(b). We must mention here that these measurements were performed with a magnetic field perpendicular to the surface of the SQUID loop. A fixed bias current of 100 nA was used in both cases. Fig. 4(b) shows the periodic oscillations in the voltage across the nano-SQUID which are rather triangular in shape as expected in the short Josephson limit.[45] Although the critical current for this SQUID was 40 μA, we have chosen a low current for the SQUID operation. The oscillation period was found to be ~0.04 T at low fields which increased slightly at higher fields, possibly due to the increase in vortex count.[46] The flux sensitivity for this nano-SQUID was found to be ~1.5 mV per flux quantum (mV/ϕ_0) at low fields. We do not observe any difference in the oscillation period in Fig. 4(b) after the SMM layer deposition. Sudden changes in the spin state of a molecular magnet can occur *via* thermal activation or *via* quantum tunneling of magnetization. The magnetic moment associated with spin state S_Z is given by $-2\mu_B S_Z$. When placed on top of a nano-SQUID, this moment threads a magnetic flux into the SQUID loop as shown in the schematic in Fig. 4(c). Any sudden change in the spin state of the molecule leads to a sudden change in the flux threading into the SQUID loop. As a SQUID device operating in a constant current bias

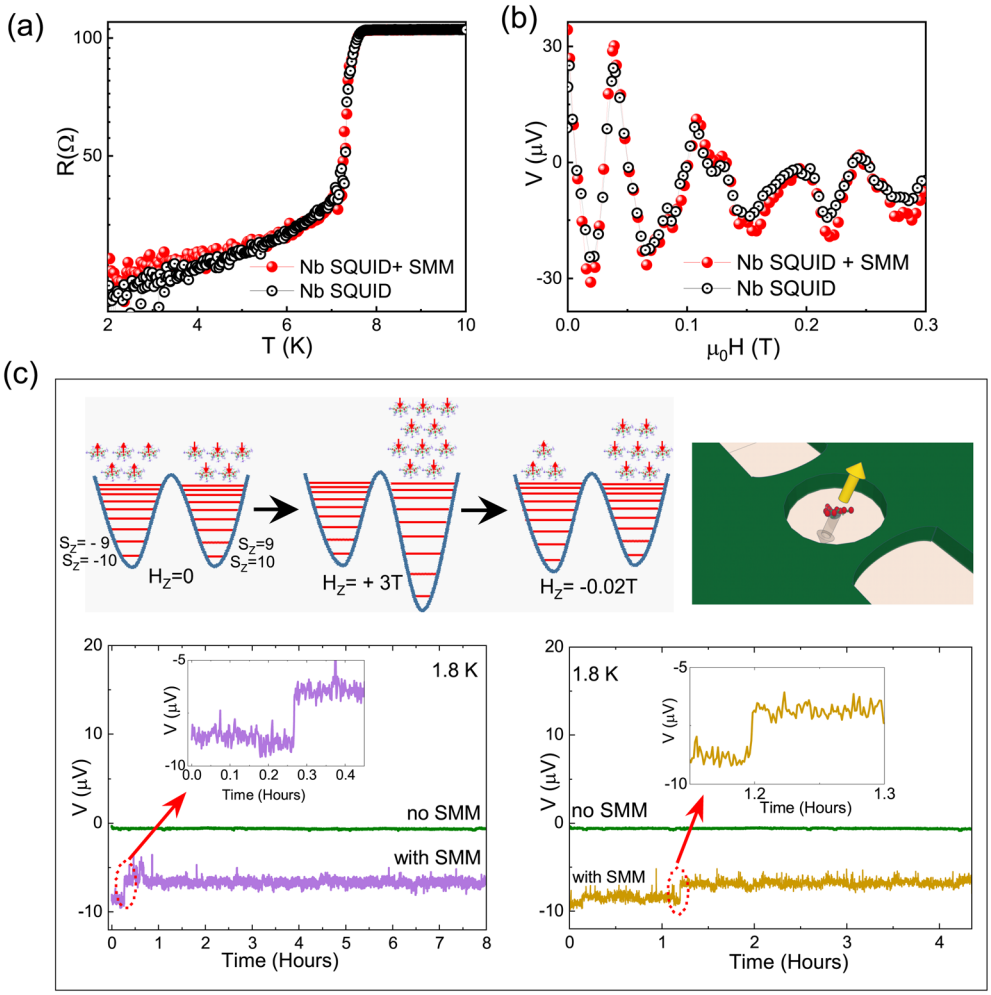

Fig. 4 (a) Comparison of zero-field $R(T)$ curves for Nb nano-SQUIDs with and without SMMs. For the same devices the magnetic field responses of voltage across the Nb nano-SQUID ($V(H)$) are compared at 2 K in panel (b). Panel (c) shows the schematic representation of the variation of distribution of SMMs in the double potential well following the magnetic field variations from the 0 T → +3 T → −0.02 T sequence used in our experiment (top left). We also show the pictorial representation of the two anisotropic moments of a Mn_{12}-ac molecule placed inside a SQUID loop (top right). Any random change in the direction of moment due to thermally assisted or quantum mechanical tunneling causes a change in the voltage across the SQUID. The bottom figures of panel (c) show the voltage across the Nb nano-SQUID with SMMs observed over a long time measured at −0.02 T after following the above sequence. We observe the jumps in the voltage at random times (in both repetitions) (bottom left and right). The magnified views of these steps are shown in the respective insets. For comparison we have also shown the voltage across a bare Nb nano-SQUID which shows no voltage jumps.

mode is a flux-to-voltage converter, a change in flux results in a change in the voltage across the SQUID. Thermally assisted, as well as quantum mechanical tunneling of magnetization in SMMs is completely random in time. Therefore, in the SMM coated nano-SQUID, random jumps in the voltage across the SQUID are a signature of the magnetization tunneling process (bottom panel of Fig. 4(c)). In this experiment, we first applied a high magnetic field (+3 T) parallel to the SMM coated nano-SQUID to magnetically saturate the Mn_{12}-ac molecules along the field direction. Subsequently, a small magnetic field was applied in the opposite direction (−0.02 T), to tilt the anisotropy barrier of the SMM which may help to trigger the magnetization tunneling process, as schematically shown in Fig. 4(c). Initially, at zero field, there is equal probability of SMMs to have magnetization in both the anisotropy directions. Upon applying a high field the double well potential tilts and most SMMs align in the field direction. When brought back to zero field some SMMs may retain this direction, which slowly relax over time. Allowing a small field in the opposite direction helps in the relaxation process which occurs through magnetization tunneling. In this condition, the voltage across the SMM coated Nb nano-SQUID was recorded over a long time (8 hours) (bottom panel of Fig. 4(c)). The entire process was carried out at a fixed temperature of 1.8 K. As shown in the bottom panel of Fig. 4(c), a step-like jump in the voltage across the nano-SQUID is apparent. On repeating the same experiment we observed more step-like jumps in the voltage at different times (bottom panel of Fig. 4(c)). In contrast, when the same experimental conditions were applied to a bare Nb nano-SQUID, no analogous voltage jumps were observed over a very long waiting

period. This background signal has been shown as a solid line marked as "no SMM" (bottom panel of Fig. 4(c)). The important noise sources that can affect the observed voltage response are (i) thermal instability and (ii) magnetic field (flux) noise. In order to rule out any thermal fluctuation-driven voltage jumps, we routinely monitor the temperature stability over the entire span of the measurements. It was found that the temperature was stable within 1 mK during the entire measurement, which is too small to generate any appreciable sudden change in the SQUID voltage. Regarding flux noise from the applied magnetic field, we would like to mention that the measurements were intentionally carried out in a magnetic field parallel to the SQUID loop (so that magnetic flux threading into the SQUID loop is negligible) to minimize flux noise effects. Additionally, the instrumental background noise level in the voltage response is an order of magnitude less than the voltage jump caused by magnetization tunneling. The observed step-like jumps in the SMM coated Nb nano-SQUID voltage can only be explained by a change in magnetic flux through the SQUID, only possible *via* the magnetization tunneling phenomenon of SMMs.

Conclusions

In conclusion, we have shown that superconducting systems can effectively sense the magnetic flux of magnetic molecules when placed in close contact. Transport measurements performed on Mn_{12}-ac coated thin superconducting Nb strips near the superconducting transition showed a clear enhancement in the activation energy of magnetic vortices. The Langmuir–Blodgett technique allowed us to form layered SMM films, albeit with a low density of SMMs. The enhanced vortex activation energy implies that the presence of magnetic molecules, even when deposited in very low density, can be detected *via* the change in resistance near the superconducting transition. We also performed transport experiments on SMM coated Nb nano-SQUIDs with very small active loops, fabricated using the FIB technique. These experiments showed a measurable voltage signal corresponding to tunneling of magnetization in SMM molecules. A sudden change in the spin state of SMMs led to a sudden change in the magnetic flux through the nano-SQUID which was detected as a jump in the voltage across the SQUID. No such jumps were observed in the SQUIDs without the SMM layer. This work shows the feasibility of hybrid spintronic devices combining superconductivity with the wide variety of available high-spin molecular magnets. For example, operating conditions of superconducting transition edge sensors[47–49] can be easily tuned by local SMM deposits on the sensor tracks. Similarly, the direct detectability of magnetization tunneling events in SMMs using ultra small nano-SQUIDs opens up the possibility of fundamental experiments on the relaxation process in a variety of SMMs.

Data availability

The data supporting this article have been included as part of the ESI,† and in the main text.

Conflicts of interest

All of the authors involved in this work declare that they have no conflicts of interest to disclose.

Acknowledgements

The authors thank the National Institute of Science Education and Research (NISER), Department of Atomic Energy, Government of India, for funding the research work through project numbers RIN-4001 and RIN-4002. We acknowledge Debashree Nayak and Dr Pratap Kumar Sahoo from NISER Bhubaneswar for carrying out AFM measurements.

References

1 L. Bogani and W. Wernsdorfer, Molecular spintronics using single-molecule magnets, *Nat. Mater.*, 2008, **7**, 179–186.
2 K. Hymas and A. Soncini, Molecular spintronics using single-molecule magnets under irradiation, *Phys. Rev. B*, 2019, **99**, 245404.
3 E. Moreno-Pineda and W. Wernsdorfer, Measuring molecular magnets for quantum technologies, *Nat. Rev. Phys.*, 2021, **3**, 645–659.
4 A. Gaita-Ariño, F. Luis, S. Hill and E. Coronado, Molecular spins for quantum computation, *Nat. Chem.*, 2019, **11**, 301–309.
5 T. Lis, Preparation, structure, and magnetic properties of a dodecanuclear mixed-valence manganese carboxylate, *Acta Crystallogr., Sect. B*, 1980, **36**, 2042–2046.
6 R. Sessoli, D. Gatteschi, A. Caneschi and M. Novak, Magnetic bistability in a metal-ion cluster, *Nature*, 1993, **365**, 141–143.
7 L. Thomas, F. Lionti, R. Ballou, D. Gatteschi, R. Sessoli and B. Barbara, Macroscopic quantum tunnelling of magnetization in a single crystal of nanomagnets, *Nature*, 1996, **383**, 145–147.
8 J. M. Hernandez, X. X. Zhang, F. Luis, J. Tejada, J. R. Friedman, M. P. Sarachik and R. Ziolo, Evidence for resonant tunneling of magnetization in Mn_{12} acetate complex, *Phys. Rev. B:Condens. Matter Mater. Phys.*, 1997, **55**, 5858–5865.
9 A. Zabala-Lekuona, J. M. Seco and E. Colacio, Single-Molecule Magnets: From Mn_{12}-ac to dysprosium metallocenes, a travel in time, *Coord. Chem. Rev.*, 2021, **441**, 213984.
10 K. Kim, D. M. Seo, J. Means, V. Meenakshi, W. Teizer, H. Zhao and K. R. Dunbar, Mn_{12}-acetate film pattern generated by photolithography methods, *Appl. Phys. Lett.*, 2004, **85**, 3872–3874.
11 K. Kim, A. Ford, V. Meenakshi, W. Teizer, H. Zhao and K. R. Dunbar, Nanopatterning of Mn_{12}-acetate single-molecule magnet films, *J. Appl. Phys.*, 2007, **102**, 094306.
12 D. Seo, V. Meenakshi, W. Teizer, H. Zhao and K. Dunbar, Enhanced magnetic anisotropy of Mn_{12}-acetate, *J. Magn. Magn. Mater.*, 2006, **301**, 31–36.
13 J. Means, V. Meenakshi, R. Srivastava, W. Teizer, A. Kolomenskii, H. Schuessler, H. Zhao and K. Dunbar,

Films of Mn_{12}-acetate deposited by low-energy laser ablation, *J. Magn. Magn. Mater.*, 2004, **284**, 215–219.
14 M. Clemente-León, H. Soyer, E. Coronado, C. Mingotaud, C. J. Gómez-García and P. Delhaès, Langmuir–Blodgett Films of Single-Molecule Nanomagnets, *Angew. Chem., Int. Ed.*, 1998, **37**, 2842–2845.
15 O. N. Oliveira Jr, L. Caseli and K. Ariga, The past and the future of Langmuir and Langmuir–Blodgett films, *Chem. Rev.*, 2022, **122**, 6459–6513.
16 K. Ariga, Don't forget Langmuir–Blodgett films 2020: interfacial nanoarchitectonics with molecules, materials, and living objects, *Langmuir*, 2020, **36**, 7158–7180.
17 G. Gabarró-Riera, G. Aromí and E. C. Sañudo, Magnetic molecules on surfaces: SMMs and beyond, *Coord. Chem. Rev.*, 2023, **475**, 214858.
18 M. Cavallini, M. Facchini, C. Albonetti and F. Biscarini, Single molecule magnets: from thin films to nano-patterns, *Phys. Chem. Chem. Phys.*, 2008, **10**, 784–793.
19 G. Serrano, L. Poggini, M. Briganti, A. L. Sorrentino, G. Cucinotta, L. Malavolti, B. Cortigiani, E. Otero, P. Sainctavit, S. Loth, *et al.*, Quantum dynamics of a single molecule magnet on superconducting Pb (111), *Nat. Mater.*, 2020, **19**, 546–551.
20 M. Bal, J. R. Friedman, K. Mertes, W. Chen, E. M. Rumberger, D. N. Hendrickson, N. Avraham, Y. Myasoedov, H. Shtrikman and E. Zeldov, Experimental upper bound on superradiance emission from Mn_{12} acetate, *Phys. Rev. B:Condens. Matter Mater. Phys.*, 2004, **70**, 140403.
21 E. Bellido, P. González-Monje, A. Repollés, M. Jenkins, J. Sesé, D. Drung, T. Schurig, K. Awaga, F. Luis and D. Ruiz-Molina, Mn_{12} single molecule magnets deposited on SQUID sensors: the role of interphases and structural modifications, *Nanoscale*, 2013, **5**, 12565–12573.
22 A. Verma, S. Verma, P. Singh and A. Gupta, Ageing effects on the magnetic properties of Mn_{12}-based acetate and stearate SMMs, *J. Magn. Magn. Mater.*, 2017, **439**, 76–81.
23 T. Senapati, A. K. Karnad and K. Senapati, Phase biasing of a Josephson junction using Rashba–Edelstein effect, *Nat. Commun.*, 2023, **14**, 7415.
24 A. G. Troeman, H. Derking, B. Borger, J. Pleikies, D. Veldhuis and H. Hilgenkamp, NanoSQUIDs based on niobium constrictions, *Nano Lett.*, 2007, **7**, 2152–2156.
25 M. José Martínez-Pérez and D. Koelle, NanoSQUIDs: Basics & recent advances, *Phys. Sci. Rev.*, 2017, **2**, 20175001.
26 J. Luomahaara, V. Vesterinen, L. Grönberg and J. Hassel, Kinetic inductance magnetometer, *Nat. Commun.*, 2014, **5**, 4872.
27 T. Van Duzer and C. W. Turner, *Principles of Superconductive Devices and Circuits*, 1981,.
28 R. F. Voss, R. B. Laibowitz and A. N. Broers, Niobium nanobridge dc SQUID, *Appl. Phys. Lett.*, 1980, **37**, 656–658.
29 C. Granata, A. Vettoliere, M. Russo and B. Ruggiero, Noise theory of dc nano-SQUIDs based on Dayem nanobridges, *Phys. Rev. B:Condens. Matter Mater. Phys.*, 2011, **84**, 224516.
30 L. Wu, X. Wang, G. Wang and G. Chen, In situ X-ray scattering observation of two-dimensional interfacial colloidal crystallization, *Nat. Commun.*, 2018, **9**, 1335.
31 C. R. Hansen, T. J. Sørensen, M. Glyvradal, J. Larsen, S. H. Eisenhardt, T. Bjørnholm, M. M. Nielsen, R. Feidenhans'l and B. W. Laursen, Structure of the Buried Metal-Molecule Interface in Organic Thin Film Devices, *Nano Lett.*, 2009, **9**, 1052–1057.
32 J. Reiche, U. Pietsch, H.-P. Fink and H. Lemmetyinen, A comparison of X-ray methods for structure refinement of Langmuir-Blodgett multilayers, *Acta Polym.*, 1992, **43**, 206–209.
33 M. Pomerantz and A. Segmüller, High resolution X-ray diffraction from small numbers of Langmuir-Blodgett layers of manganese stearate, *Thin Solid Films*, 1980, **68**, 33–45, Special Issue on Langmuir-Blodgett Films.
34 M. del Carmen Giménez-López, F. Moro, A. La Torre, C. J. Gómez-García, P. D. Brown, J. Van Slageren and A. N. Khlobystov, Encapsulation of single-molecule magnets in carbon nanotubes, *Nat. Commun.*, 2011, **2**, 407.
35 A. Gubin, K. Il'in, S. Vitusevich, M. Siegel and N. Klein, Dependence of magnetic penetration depth on the thickness of superconducting Nb thin films, *Phys. Rev. B:Condens. Matter Mater. Phys.*, 2005, **72**, 064503.
36 C. Delacour, L. Ortega, M. Faucher, T. Crozes, T. Fournier, B. Pannetier and V. Bouchiat, Persistence of superconductivity in niobium ultrathin films grown on R-plane sapphire, *Phys. Rev. B:Condens. Matter Mater. Phys.*, 2011, **83**, 144504.
37 N. Pinto, S. J. Rezvani, A. Perali, L. Flammia, M. V. Milošević, M. Fretto, C. Cassiago and N. De Leo, Dimensional crossover and incipient quantum size effects in superconducting niobium nanofilms, *Sci. Rep.*, 2018, **8**, 4710.
38 X.-Z. Duan and Z.-H. He, Normal State Properties and Upper Critical Magnetic Field in Three-dimensional Polycrystalline Niobium Films, *J. Supercond. Novel Magn.*, 2021, **34**, 2517–2522.
39 T. T. M. Palstra, B. Batlogg, R. B. van Dover, L. F. Schneemeyer and J. V. Waszczak, Dissipative flux motion in high-temperature superconductors, *Phys. Rev. B:Condens. Matter Mater. Phys.*, 1990, **41**, 6621–6632.
40 H. Zhang, Y. Fang, T. Wang, Y. Liu, J. Chu, Z. Li, D. Jiang, G. Mu, Z. Di and F. Huang, Anisotropic thermally activated flux-flow behavior in the layered superconductor 2M-WS_2, *Phys. Rev. B*, 2021, **103**, L180503.
41 H.-F. Zhang, X.-H. Chen, Q.-L. Xiao, F. Chen, Z. Feng, S. Cao, J. Zhang, Y. Qi, Z. Shi and J.-Y. Ge, Evolution of superconducting properties in $Fe_{1.1}Se_{0.8}Te_{0.2}$ films before and after structure avalanche, *ACS Appl. Mater. Interfaces*, 2021, **13**, 42138–42145.
42 P. Pratap, L. Nanda, K. Senapati, R. Aloysius and V. Achanta, Optimization of the superconducting properties of NbTiN thin films by variation of the N_2 partial pressure during sputter deposition, *Supercond. Sci. Technol.*, 2023, **36**, 085017.
43 H. K. Kundu, K. R. Amin, J. Jesudasan, P. Raychaudhuri, S. Mukerjee and A. Bid, Effect of dimensionality on the

vortex dynamics in a type-II superconductor, *Phys. Rev. B*, 2019, **100**, 174501.

44 A. Banerjee, A. Mohapatra, R. Ganesan and P. A. Kumar, Restoring superconductivity in the quantum metal phase of $NbSe_2$ using dissipative coupling, *Nano Lett.*, 2019, **19**, 1625–1631.

45 K. Hasselbach, D. Mailly and J. Kirtley, Micro-superconducting quantum interference device characteristics, *J. Appl. Phys.*, 2002, **91**, 4432–4437.

46 J. Ku, Z. Yoscovits, A. Levchenko, J. Eckstein and A. Bezryadin, Decoherence and radiation-free relaxation in Meissner transmon qubit coupled to Abrikosov vortices, *Phys. Rev. B*, 2016, **94**, 165128.

47 K. D. Irwin and G. C. Hilton, Transition-edge sensors, *Cryogenic Particle Detection*, 2005, pp. 63–150.

48 J. E. Sadleir, S. J. Smith, S. R. Bandler, J. A. Chervenak and J. R. Clem, Longitudinal proximity effects in superconducting transition-edge sensors, *Phys. Rev. Lett.*, 2010, **104**, 047003.

49 J. E. Sadleir, S. J. Smith, S. R. Bandler, J. S. Adams, S. E. Busch, M. E. Eckart, J. A. Chervenak, R. L. Kelley, C. A. Kilbourne, F. S. Porter, *et al.*, Magnetically tuned superconducting transition-edge sensors, *IEEE Trans. Appl. Supercond.*, 2013, **23**, 2101405.